Synthesis of lauryl methacrylate and poly(ethylene glycol) methyl ether methacrylate copolymers with tunable microstructure and emulsifying properties

Agustín Iborra, Lucas Salvatierra, Juan M. Giussi, Omar Azzaroni

PII: S0014-3057(19)30046-1
DOI: https://doi.org/10.1016/j.eurpolymj.2019.04.010
Reference: EPJ 8974

To appear in: *European Polymer Journal*

Received Date: 8 January 2019
Revised Date: 4 April 2019
Accepted Date: 5 April 2019

Please cite this article as: Iborra, A., Salvatierra, L., Giussi, J.M., Azzaroni, O., Synthesis of lauryl methacrylate and poly(ethylene glycol) methyl ether methacrylate copolymers with tunable microstructure and emulsifying properties, *European Polymer Journal* (2019), doi: https://doi.org/10.1016/j.eurpolymj.2019.04.010

Synthesis of lauryl methacrylate and poly(ethylene glycol) methyl ether methacrylate copolymers with tunable microstructure and emulsifying properties

Agustín Iborra,[1] Lucas Salvatierra,[1,2] Juan M. Giussi,[1*] and Omar Azzaroni[1]

[1]*Instituto de Investigaciones Fisicoquímicas Teóricas y Aplicadas (INIFTA) – Departamento de Química – Facultad de Ciencias Exactas - Universidad Nacional de La Plata – CONICET – (1900) La Plata – Argentina.*

[2]*Facultad de Química e Ingeniería, Pontificia Universidad Católica Argentina – (2000) Rosario - Argentina.*

Abstract

In this work we study the synthesis and properties of copolymers constituted of lauryl methacrylate and poly(ethylene glycol) methyl ether methacrylate monomers, prepared by atom transfer radical copolymerization in the entire composition range (with low and high monomer conversion). We propose a description of the copolymer microstructure, and evaluate the composition drift effect in the thermal and solution properties of the obtained copolymers. Nuclear magnetic resonance (NMR) was used to determine the chemical composition of the copolymers, while differential scanning calorimetry and themogravimetric analysis was employed to understand the thermal chracteristics. Rheological studies were conducted to obtain the viscosity and viscoelastic properties that were correlated with thermal transitions at different temperatures. Finally, dynamic light scattering (DLS) and surface tension measurements were used to evaluate the copolymer solution properties. The incorporation of an oil phase in the self-assembled aggregates was evaluated by DLS and characterized by atomic force microscopy, diffusion-ordered spectroscopy NMR and nuclear Overhauser effect NMR spectroscopy.. Our results suggest a longer sequence of LMA units in the copolymer chain and a drift effect in the case of high monomer conversions. A clear dependence on copolymer composition and microstructure to disperse an oil phase in water was observed. We believe that these results bring valuable knowledge that advances the field of macrosurfactants as well as their potential applications in oil recovery and other industrial processes.

Keywords: Amphiphilic copolymers; Microstructural changes; Macrosurfactant; Thermal and rheological properties; Emulsifying Capacity.

*Corresponding author: jmgiussi@inifta.unlp.edu.ar

INTRODUCTION

Emulsions, generally formed by the dispersions of an oil phase in water, play a key role in many industrial processes. Coatings,[1–3] cosmetics,[4,5] food,[6–8] electronics,[9,10] and petroleum recovery[11–14] are only some examples of the applications of these compatibility systems. The use of amphiphilic copolymers has improved several aspects of low-molecular-weight surfactants.[15–18] For instance, polymeric surfactants have lower critical micelle concentrations and lower diffusion coefficients than traditional surfactants do.[19–21] On the other hand, the use of low-molecular-weight surfactants with high amphiphilic properties is limited to ionic entities containing ionic functional groups at their head, such as sulfonates, phosphates, or quaternary ammonium salts.

The need to prepare molecules with two domains exhibiting different polarity has traditionally turned block copolymers into the most frequently used amphiphilic systems.[22–25] This is also explained by the fact that their synthetic methods are well-established, and, on the other hand, because of their topology, they are tunable and adaptive.

Some authors have described the preparation and use of statistical copolymers with amphiphilic properties. Some of them have used free-radical copolymerization of monomers with long polar and nonpolar pendant groups.[26–32] This type of procedure generates a linear backbone with a hydrophilic and hydrophobic polymeric pendant group statistically distributed along the backbone. More recently, different research groups have begun to use controlled radical copolymerization techniques to attain amphiphilic copolymer with better control over composition, molecular weight, and polydispersity.[33–36] The most relevant difference between the traditional block copolymers and the aforementioned statistical copolymers is that block copolymers display well-defined, separated hydrophilic and hydrophobic domains. This feature facilitates self-assembly and produces dispersions with monodisperse size and morphology. Even though hydrophilic/hydrophobic statistical copolymers do not display this topological features, they have demonstrated potential capabilities as emulsifying agents to generate disperse systems similar to Pickering emulsions.

Moreover, variations in composition and copolymer microstructure can produce various changes in the final properties, which are of great relevance in terms of material performance and function.[37–39] The preparation of copolymers at low monomer conversions can help in the prediction and distribution along the copolymer chain,[40] and could only be extrapolated to high concentrations by setting the monomer composition in the feed for controlled copolymerization methods. In general, this extrapolation contains many errors.

The rheological characteristics of low-molecular-weight surfactants are strongly affected at high temperatures. Along these lines, some authors have proposed the combination of some useful properties of polymeric materials with those of traditional surfactants.[41–44] While considerable

research efforts have been devoted to the study of the rheological properties of polymer surfactants, low surfactant concentrations and their stability have received little attention.[45–47]

In a previous work,[31] with the use of free-radical copolymerization, we designed and prepared amphiphilic copolymers for use as emulsifying agents with lauryl methacrylate (LMA) and poly (ethylene glycol) methyl ether methacrylate (PEGMA) as constituting monomer units. Their amphiphilic characteristics allowed us to disperse an organic phase in water and to disperse and stabilize carbon nanotubes in aqueous solutions. While, various studies deal mostly with PEGMA-based copolymers and their thermoresponse characteristics,[48,49] a systematic study on this monomer pair in the entire composition range is still missing.

Understanding the influence of the microstructure on the properties of amphiphilic copolymer remains a key issue in the development of this type of systems. Therefore, the aim of this work was to design, prepare and characterize LMA- and PEGMA-based copolymers in their entire composition range with low and high monomer conversion. We aim to describe the copolymer microstructure of the LMA-PEGMA pair, and to evaluate the composition drift effect in the thermal and solution properties of the obtained copolymers. Additionally, we intended to find the best composition and copolymer microstructure to emulsify and disperse an oil phase in water. To meet these goals, we used atom transfer radical copolymerization under different experimental conditions to attain monomer conversions below 25% and above 85% for the entire composition range. Nuclear magnetic resonance (NMR) was used to determine the chemical composition of the copolymers obtained. Differential scanning calorimetry (DSC) and themogravimetric analysis (TGA) helped to explain the thermal transition and decomposition profiles. Rheological studies were conducted to obtain the viscosity and viscoelastic properties that were compared to thermal transition by variation of temperature. Finally, the incorporation of an oil phase in the self-assembled aggregates was evaluated by DLS and characterized by Atomic Force Microscopy, Diffusion-Ordered Spectroscopy NMR, Nuclear Overhauser Effect NMR spectroscopy, and Atomic Force Microscopy.

These results contribute to improve our understanding of the microstructure-property relationship in amphiphilic copolymers. We believe that they provide fundamental knowledge about the capabilities of these emulsifying agents for potential use in oil recovery and other industrial applications

EXPERIMENTAL

Materials

Monomers, lauryl methacrylate (LMA, 96% Aldrich) and poly(ethylene glycol) methyl ether methacrylate (PEGMA, average Mn 500 Aldrich) were distilled under reduced pressure before use. The initiator, Ethyl α-bromoisobutyrate (EBIB, 98% Aldrich), CuBr (99.995% Aldrich), $CuBr_2$ (99.995% Aldrich), N,N,N′,N″,N″-Pentamethyldiethylenetriamine (PMDETA, 99% Aldrich), and the solvents (THF (RPE, Anedra) and methanol (RPE, Anedra)) were used as received. The dialysis tubing cellulose membrane with a typical molecular weight cut-off of 14,000 was provided by Aldrich.

Polymerization

LMA_x-$PEGMA_y$ copolymers, where *x* is the LMA molar fraction in the feed and *y* the PEGMA molar fraction in the feed, respectively, were synthesized by Atom Transfer Radical Polymerization (ATRP) using EBIB as initiator and Copper/PMDETA as catalyst. To obtain different monomer conversions, two synthesis conditions were applied.

Condition 1. 20 mmol of LMA_x-$PEGMA_y$ monomer mixture (table S1) was introduced into a Schlenk tube. The mixture was purged with N_2 bubbles at 0 °C for 30 minutes. Then 0.22 mmol (38.5 mg) of PMDETA and 0.02 mmol of $CuBr_2$ (4.5 mg) were added and the purge was continued for 15 minutes. Then 0.2 mmol of CuBr (28.7 mg) was incorporated and the mixture was sonicated under N_2 in an ice bath for 10 minutes. Afterwards, the tube was heated at 40 ºC and 0.2 mmol of EBIB (39 mg) was introduced to start the reaction (Monomer/Initiator ratio of 100). After 5 minutes, $LMA_{0.2}$-$PEGMA_{0.8}$, $LMA_{0.4}$-$PEGMA_{0.6}$ and $LMA_{0.6}$-$PEGMA_{0.4}$ were added in 20 mL of water and the LMA monomer was eliminated by extraction with toluene (3x10mL) without agitation. The aqueous phase, along with the copolymers, was purified by dialysis and freeze-dried. $LMA_{0.8}$-$PEGMA_{0.2}$ was precipitated in methanol and purified with a two-step dissolution process in THF and precipitation in methanol, centrifuged, and dried under vacuum. The absence of olefinic protons in the H NMR spectra confirmed polymers purity (figure S1).

Condition 2. 20 mmol of LMA_x-$PEGMA_y$ monomer mixture (table S1) was introduced into a Schlenk tube. The mixture was purged with N_2 bubbles at 0 °C for 30 minutes. Then 0.2 mmol (35 mg) of PMDETA was incorporated and the purge was continued for 15 minutes. Then 0.2 mmol of CuBr (28.7 mg) was introduced and the mixture was sonicated under N_2 in an ice bath for 10 minutes. Afterwards, the tube was heated at 70 ºC and 0.2 mmol of EBIB (39 mg) was added to start the reaction (Monomer/Initiator ratio of 100). After 20 minutes, LMA_0-$PEGMA_1$ (Poly-PEGMA)

was introduced in 20 mL of water and purified by dialysis and freeze-dried. $LMA_{0.2}$-$PEGMA_{0.8}$, $LMA_{0.4}$-$PEGMA_{0.6}$ and $LMA_{0.6}$-$PEGMA_{0.4}$ were introduced in 20 mL of water and, as in the previous cases, the LMA monomer was eliminated by extraction with toluene (3x10mL) without agitation. The aqueous phase, along with the copolymers, was purified by dialysis and freeze-dried. Finally, $LMA_{0.8}$-$PEGMA_{0.2}$ and LMA_1-$PEGMA_0$ (Poly-LMA), were precipitated in methanol and purified with a two-step dissolution process in THF and precipitation in methanol, centrifuged, and dried under vacuum. The absence of olefinic protons in the H NMR spectra confirmed polymers purity (figure S1).

Characterization

Characterization and copolymer composition were estimated using Proton Nuclear Magnetic Resonance (H-NMR). Spectra were recorded on a 600 MHz Bruker Spectrometer. Self-assembled aggregates were studied by Diffusion-Ordered Spectroscopy NMR (DOSY-NMR) and Nuclear Overhauser Enhancement Spectroscopy (NOESY-NMR). The experiments were carried out on the aggregates pre-formed with $LMA_{0.6}$-co-$PEGMA_{0.4}$ copolymers from condition 1 and condition 2. For this purpose, 2% of toluene were dispersed in deuterated water solutions of 10 mg/mL of each $LMA_{0.6}$-co-$PEGMA_{0.4}$.

The average molecular weight and molecular weight distribution were determined by SEC in a LKB-2249 instrument at 25 °C. A series of four μ-Styragel columns (10^5, 10^4, 10^3, 100 Å pore size) were used with tetrahydrofuran as eluent. Polymer concentration was 5 mg/mL, and flow rate was 0.5 mL/min. The polymer was detected by infrared (IR) absorption at 5.75 μm with a Miram IA spectrophotometer detector. Poly methyl methacrylate standards supplied by Polymer Laboratories and Polysciences Inc. were used for calibration.

The thermal properties were evaluated by Differential Scanning Calorimetry (DSC) and Thermo Gravimetric Analysis (TGA). DSC measurements were performed using a DSC Q2000 (TA Instruments) under a nitrogen atmosphere at 10 °C/min heating and cooling rates, from -70 to 150°C. Three heating/cooling cycles were run to eliminate thermal prehistory. TGA analyses were performed using a TGA Q500 (TA Instruments). The equipment was kept under a nitrogen atmosphere from room temperature to 700 ºC, and a 60 ml/min purge gas was introduced.

Rheological studies of LMA_x-co-$PEGMA_y$ copolymers and their homopolymers in neat condition (without any solvent) were undertaken in a DHR-3 Rheometer (TA Instruments), using a 40 mm diameter stainless steel parallel plate and a Peltier system, working in oscillatory shear and flow mode. For all samples, the gap between the geometry and the Peltier was 1000 μm. The Linear

Viscoelastic Region (LVR) was determined in each type of sample through a strain sweep at 1 Hz. As LVR was kept beyond 100 % of strain, 1 % was used in all the oscillatory experiments. Temperature ramps at 2 ºC/min were performed between -5 ºC and around 100 ºC, at a frequency of 1 Hz. At fixed temperatures, during the first run-up, frequency scans between 0.1 Hz and 100 Hz were also conducted. Flow viscosity was obtained at the same temperatures after oscillatory tests. Data was further analyzed through the behavior of the storage modulus G', the loss modulus G'', and the loss tangent, tan δ = G''/G'. Zero-shear viscosity was obtained by steady-state shear flow at very low shear stress and compared to oscillation tests at low angular frequency. The Time Temperature Superposition (TTS) principle was applied using the embedded analysis package included in the Trios^{TM} software. Master curves using William-Landel-Ferry (WLF) model, were obtained and compared to the original data. The activation energy from Arrhenius model was also analyzed.

Solution properties were evaluated by dynamic light scattering (DLS) (Zetasizer Nano Z, laser wavelength 632 nm). The analysis of DLS and size results were carried out through distribution fit. The viscosity value used was pure water value at measurement temperatures. Polymer concentration was 1g.L^{-1}. Some emulsification studies incorporating 2% of toluene to some copolymer solutions were performed.

The surface tensions of aqueous surfactant solutions were determined by the Du Noüy ring method using an Attension Sigma 700 (Biolin Scientific) at 25 °C. The surface tensions of several solutions were measured at different concentrations. The critical micelle concentration (CMC) of surfactants was obtained from log plots of surface tension versus surfactant concentration.

The atomic force microscopy (AFM) topography images of individual aggregates of the copolymers obtained were measured with a Multimode Atomic Force Microscope (Veeco Metrology Group) in tapping mode using silicon cantilevers (Bruker) Model TESP-V2. Samples were prepared by deposition of a water dispersion drop on a silicon substrate. Then they were frozen with liquid nitrogen and freeze-dried.

RESULTS AND DISCUSSION

Copolymer synthesis and characterization

We employed two synthetic conditions. Under *condition 1*, we obtained conversion in less than 25% in order to describe the copolymer microstructure. Under *Condition 2*, we obtained higher monomer conversion and achieved more profitable conditions. In this context, both situations produced copolymers based on lauryl methacrylate (LMA) and poly(ethylene glycol) methyl ether methacrylate (average Mn 500) (PEGMA) (LMA_x-$PEGMA_y$). The structure is represented in Figure

1. Figure 1 also shows the H NMR spectra (in chloroform) for LMA_x-$PEGMA_y$ copolymers obtained using 20% Cu^{II}, 5 min of reaction time, and 40 °C of reaction temperature (condition 1). In the spectra, all resonance signals were assigned.

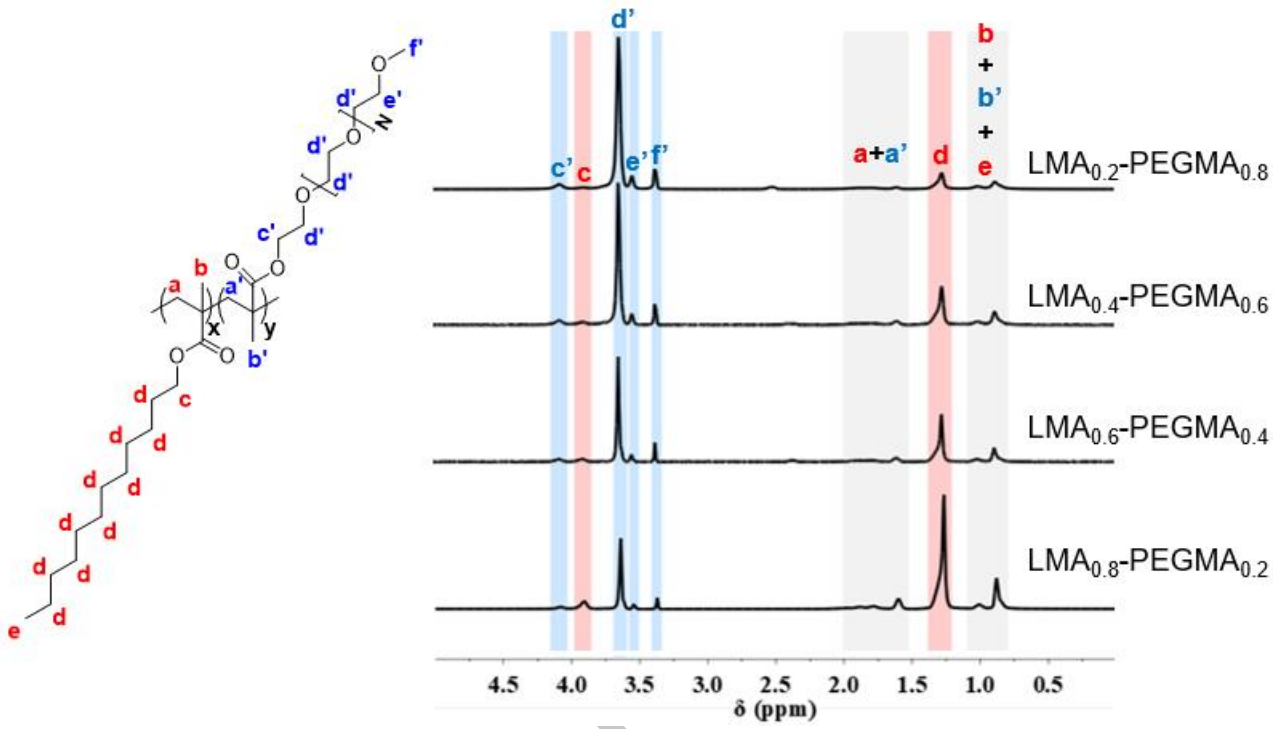

Figure 1. Generic copolymers LMA_x-$PEGMA_y$ structure and their H NMR spectra (in chloroform) using 20% Cu^{II}, 5 min of reaction time, and 40 °C of reaction temperature.

Copolymer compositions were estimated form H NMR spectra using the integral ratio of the peak at δ=1.27 corresponding to signal "*d"* of LMA monomer and the signal at δ=3.75 corresponding to signal "*d'* " of PEGMA monomer using Equation 1.

$$F_{LMA} = \frac{I^d/_{20}}{I^d/_{20} + I^{c\prime}/_{2}} \quad (1)$$

F_{LMA} represents the LMA molar fraction of the copolymers. The application of equation 1 to calculate F_{LMA} for all copolymers is shown in Table 1. Each copolymer is represented as LMA_x-co-$PEGMA_y$, where *x*, is the monomer mole fraction in the initial mixture (feed) of LMA monomer and *y*, is the monomer mole fraction in the initial mixture of PEGMA monomer. Table 1 also indicates the monomer conversion in each reaction, the weight-average molecular weight (Mw), number-average molecular weight (Mn), and the polydispersity index (PDI) of the copolymers synthesized.

Figure S2 displays the elugrams of all the polymers obtained. The increment of Mw, Mn and PDI with LMA content is due to the increase of the hydrodynamic volume of the copolymers in THF.

Table 1. Monomer conversion, mole fraction in the feed (f_{LMA}), molar fraction in the copolymer (F_{LMA}), weight-average molecular weight (Mw), number-average molecular weight (Mn), and polydispersity index (PDI) for the copolymers synthesized under condition 1 (20% CuII, 40 °C of reaction temperature and 5 minutes of reaction time) and condition 2 (0% CuII, 70 °C of reaction temperature and 20 minutes of reaction time).

Conditions	**Copolymer**	**Conv (%)***	**f_{LMA}**	**F_{LMA}****	**Mw (g/mol)**	**Mn (g/mol)**	**PDI**
20%CuII 40°C 5 min	$LMA_{0.2}$-$PEGMA_{0.8}$	23	0.2	0.28±0.03	10,300	8,400	1.22
	$LMA_{0.4}$-$PEGMA_{0.6}$	22	0.4	0.52±0.02	18,200	13,500	1.35
	$LMA_{0.6}$-$PEGMA_{0.4}$	25	0.6	0.70±0.02	30,850	18,600	1.66
	$LMA_{0.8}$-$PEGMA_{0.2}$	19	0.8	0.85±0.01	19,650	16,000	1.23
0%CuII 70°C 20 min	LMA_0-$PEGMA_1$	93	0	0±0	11,900	9,700	1.23
	$LMA_{0.2}$-$PEGMA_{0.8}$	89	0.2	0.20±0.02	70,650	34,450	2.05
	$LMA_{0.4}$-$PEGMA_{0.6}$	91	0.4	0.37±0.02	23,650	17,050	1.38
	$LMA_{0.6}$-$PEGMA_{0.4}$	93	0.6	0.53±0.01	27,600	17,400	1.58
	$LMA_{0.8}$-$PEGMA_{0.2}$	87	0.8	0.78±0.01	66,450	33,950	1.95
	LMA_1-$PEGMA_0$	88	1	1±0	90,650	68,450	1.32

* Conversions were determined by gravimetry as weight of polymer obtained /weight of monomer in the feed.

** Errors were estimated by integrating 5 times the selected signals in the NMR spectra.

The comonomer-copolymer composition curve for condition 1 is illustrated in Figure 2. The plot shows that LMA composition in the copolymer is always higher than in the feed. Following a general description, this plot would suggest a longer sequence of LMA units in the copolymer chain, as it has already been reported [40,50,51] and is evidenced by DSC. Based on the previous suggestion for the copolymers prepared under condition 2, 0% of Cu^{II}, 70 °C and 20 minutes of reaction time, a drift effect should be observed, especially for $LMA_{0.2}$-$PEGMA_{0.8}$ and $LMA_{0.8}$-$PEGMA_{0.2}$ copolymers. This is explained by the fact that, even though, in the early stages of copolymerization, LMA is the most reactive monomer, in these early stages, the monomer with the lowest yield becomes depleted sooner. LMA monomer is incorporated faster, and the copolymer is richer in the LMA monomer. When the LMA monomer is depleted, more PEGMA monomer segments are added.

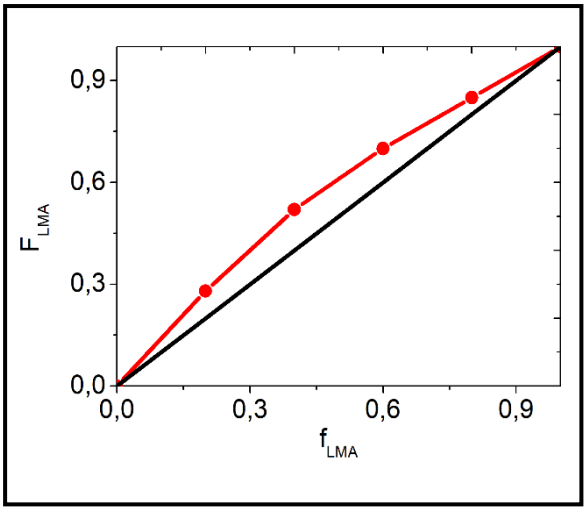

Figure 2. Comonomer-copolymer composition curve corresponding to 20% Cu^{II}, 5 min and 40 °C of reaction conditions.

Thermal Characterization

The thermal decomposition of the synthesized copolymers is shown in Figure 3. As it can be noticed, only one thermal event is observed for all samples. Depending on the initial temperature of degradation, the copolymers synthesized under condition 1 showed the following thermal stability order, $LMA_{0.8}$-$PEGMA_{0.2}$ > $LMA_{0.2}$-$PEGMA_{0.8}$ > $LMA_{0.4}$-$PEGMA_{0.6}$ > $LMA_{0.6}$-$PEGMA_{0.4}$. As regards copolymers under condition 2, despite presenting higher initial degradation temperature than their analogues under condition 1, the thermal stability order remained the same, $LMA_{0.8}$-$PEGMA_{0.2}$ (similar to the LMA homopolymer) > $LMA_{0.2}$-$PEGMA_{0.8}$ (similar to the PEGMA homopolymer)> $LMA_{0.4}$-$PEGMA_{0.6}$ > $LMA_{0.6}$-$PEGMA_{0.4}$.

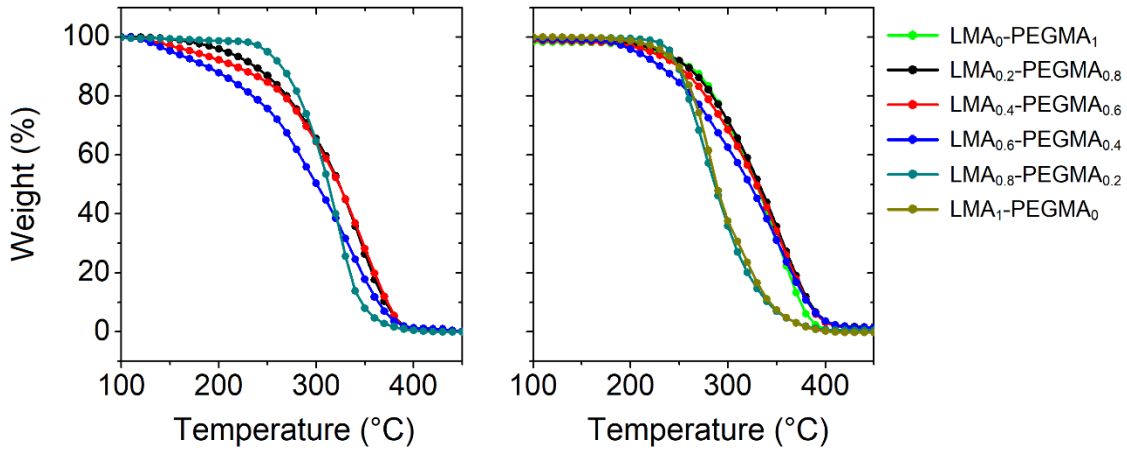

Figure 3. TGA curves for LMA-PEGMA systems at 20% Cu^{II} 5 min and 40 °C (left), and 0% Cu^{II}, 20 min, 70 °C (right). LMA_0-$PEGMA_1$ (flour green, - •-), $LMA_{0.2}$-$PEGMA_{0.8}$ (black, - •-), $LMA_{0.4}$-$PEGMA_{0.6}$ (red, - •-), $LMA_{0.6}$-$PEGMA_{0.4}$ (blue, - •-), $LMA_{0.8}$-$PEGMA_{0.2}$ (light blue, - •-), LMA_1-$PEGMA_0$ (brown, - •-).

The pair of monomers used presented complex thermal characteristics. As already known, the glass transition temperature of the PEGMA homopolymer is around -60 °C, and its melting temperature around -5 °C (Figure S3). On the other hand, the LMA homopolymer showed a glass transition temperature close to -45 °C and no melting peaks related to side-chain crystallinity due to the presence of lauryl groups (Figure S3). The copolymerization of these monomers resulted in systems with unpredictable thermal properties, shown in Figure 4. As regards condition 1 (figure 4, left), systems without composition drift, the copolymers did not present melting peaks and, except for $LMA_{0.2}$-$PEGMA_{0.8}$, which showed only one glass transition temperature, two glass transition temperatures were observed. The values of these transition temperatures were close to the glass transition temperature of PEGMA at -65 °C and the glass transition temperature of LMA at -30 °C. The presence of two thermal transitions could be indicative of microphase separation in the copolymer.

As far as condition 2 is concerned (figure 4, right), the situation is even more complex and interesting, except for $LMA_{0.8}$-$PEGMA_{0.2}$, with a glass transition temperature of approximately -33 °C, $LMA_{0.6}$-$PEGMA_{0.4}$ and $LMA_{0.4}$-$PEGMA_{0.6}$ showed a glass transition temperature of -65°C, corresponding to PEGMA glass transition temperature. On the other hand, melting peaks at around -32°C were observed. These melting peaks, corresponding to PEGMA segments, did not allow to see the glass transition temperature of LMA entities in the copolymer chains. Lastly, $LMA_{0.2}$-$PEGMA_{0.8}$ showed all transition temperatures: PEGMA glass transition temperature at -65°C, LMA glass transition temperature at -33°C, and PEGMA melting at -9°C.

The presence of two Tg values could be an indication of microphases separation in the copolymer, these transitions being dependent on the composition of the copolymers. In the case of condition 2, the composition drift helped in the melting process due to the closeness of PEGMA chains.

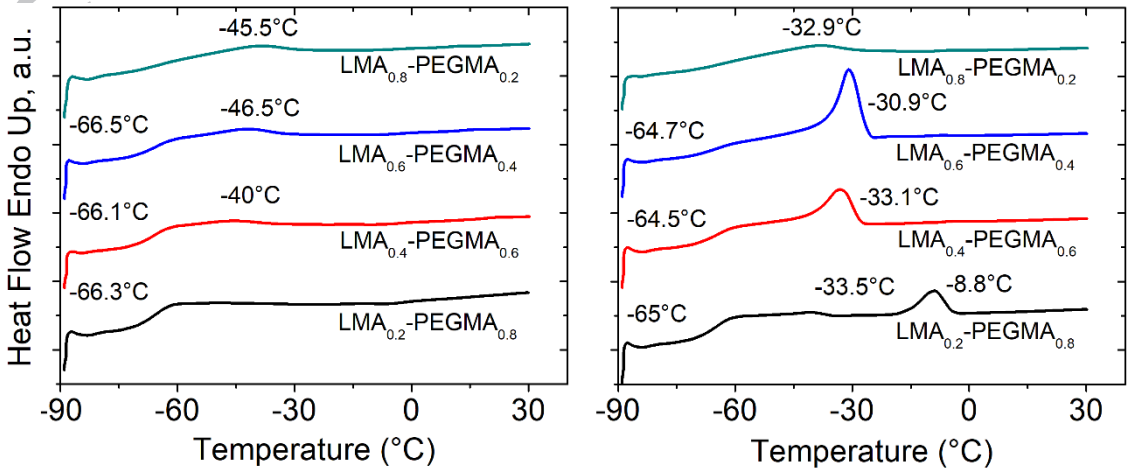

Figure 4. DSC curves of third heating cycle for LMA-PEGMA systems at 20% Cu^{II} 5 min and 40 °C (left), and 0% Cu^{II}, 20 min, 70 °C (right). $LMA_{0.2}$-$PEGMA_{0.8}$ (black, - •-), $LMA_{0.4}$-$PEGMA_{0.6}$ (red, - •-), $LMA_{0.6}$-$PEGMA_{0.4}$ (blue, - •-), $LMA_{0.8}$-$PEGMA_{0.2}$ (light blue, - •-).

Rheological Behavior

Rheometry is one of the most important methods to describe the viscous and viscoelastic properties of polymers. In order to better understand and clarify the complex transition determined by DSC, the samples obtained under condition 2 were analyzed with this technique. The oscillatory tests allowed us to compare the different dynamics of PEGMA and LMA homopolymers, as well as their fingerprints in the different copolymer fractions. As temperature sweeps were restricted to 0-100 ºC, the Time-Temperature Superposition (TTS) principle was a great value tool to spread both the minimum and maximum of temperature and frequency. As an example, Figure 5, left, shows the application of TTS to the PEGMA homopolymer, by performing frequency sweeps at different temperatures and obtaining the shift factors. The WLF model was applied to assemble a master curve that spanned in a wider range (see the modelled curve at 20 ºC and its perfect matching with the original one). In addition, measured temperature sweeps (G', G'', and tan δ) were compared to the predicted responses for all the samples using the TTS-WLF model, yielding excellent results (e.g., Figure 5, right), mainly at lower temperatures where $Tg < T < Tg+100K$, even for both homopolymers: PEGMA or LMA.

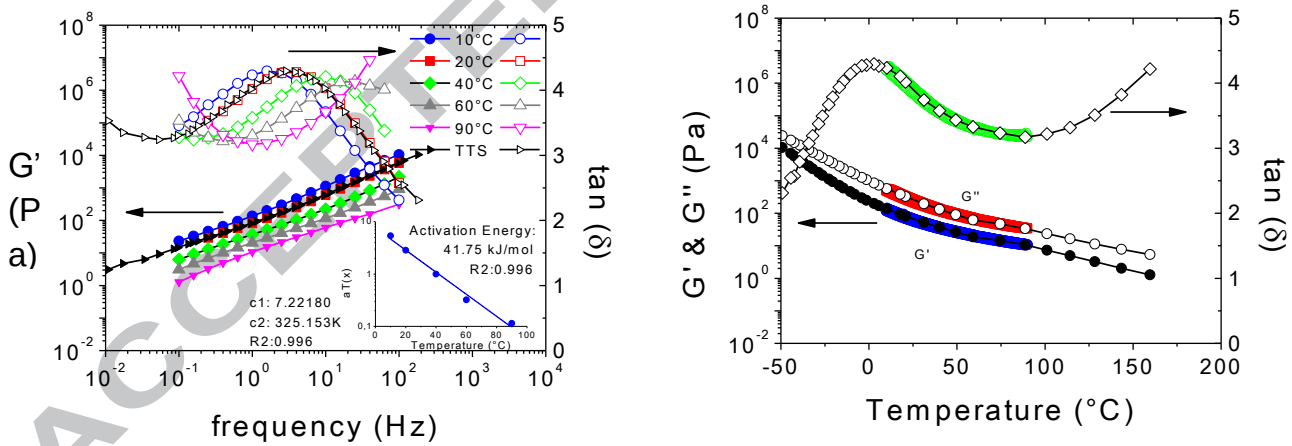

Figure 5. PEGMA homopolymer (f_{LMA} = 0). Left: Frequency sweeps at different temperatures and 1 % strain, with a superimposed master curve at 20 ºC generated by the TTS, modeling with a WLF and Arrhenius equation (see insert). Right: Temperature ramp at 2 º/min, 1 Hz and 1 %. G', G'' and tan (δ) in the original range between 5 ºC and 90 ºC and the extended range through the predicted curve by TTS and WLF.

Figure 6 displays a tan (δ) comparison for all samples synthesized under condition 2. As it can be observed (see also Figure 5, right), PEGMA homopolymer has a low temperature peak in tan (δ) associated with the melting of its crystalline zones as measured by DSC (see Figure S3).

On the other hand, the pure LMA homopolymer, mainly amorphous, has a huge damping peak around 70 ºC with a tan (δ) value close to 100 (i.e., G'' is two orders higher than G'). This relaxation has not been previously reported for the LMA monomer polymerized by ATRP. This could be ascribed to high temperature rearrangements and cooperative movements of lauryl side chains assisting a local flow of the main chain. On the contrary, DSC did not show any change in the baselines around this temperature (not shown in Figure 4), nor any sign of melting at lower temperatures, related to the side-chain crystallinity of these lauryl groups. Moreover, for the pure LMA homopolymer, the absence of a visible side chain crystallinity could also be related to the tacticity of the obtained polymer. For copolymers, this behavior could be even more hindered by PEGMA units, thereby preventing lauryl packing. These unexpected features could be the platform for further research.

The copolymers of condition 2 with a higher LMA fraction ($LMA_{0.8}$-$PEGMA_{0.2}$ and $LMA_{0.6}$-$PEGMA_{0.4}$) showed mixed and transitional behavior within LMA and PEGMA. The pattern of $LMA_{0.4}$-$PEGMA_{0.6}$ and $LMA_{0.2}$-$PEGMA_{0.8}$ was similar to that of PEGMA homopolymer, as also predicted and identified by DSC (Figure 4, right, and Figure S3).

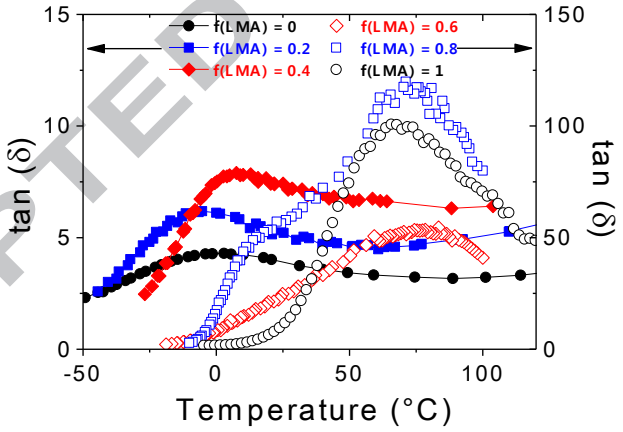

Figure 6. TTS temperature modeled patterns in tan (δ) for both homopolymers (PEGMA, black filled circles; and LMA: black open circles) and copolymers fractions of LMA of condition 2 (f_{LMA}= 0.2: blue filled squares; f_{LMA}= 0.4: red filled diamonds; f_{LMA}= 0.6: red open diamonds; and f_{LMA}= 0.8: blue open squares).

Figure 7 shows the behavior of the zero-shear viscosity (related to Mw, see Table 1) and the activation energy of both relaxation processes from Figure 6 obtained through Arrhenius modeling (see, for example, inset in Figure 5, left), as a function of the LMA fraction. Homopolymer and copolymer viscosities ranged from 100 to 5000 Pa.s at 20 ºC, a consistency similar to that of molasses and polymer melts. Their values remained constant up to f_{LMA} around 0.6, from which an

abrupt increase was observed. In addition, these samples with higher LMA content showed a Newtonian behavior up to 10 /s of shear rate; and an increasing shear-thinning effect in viscosity was detected as the PEGMA fraction dominated.

Finally, the activation energy from the relaxation processes observed in Figure 6 showed the transition between pure PEGMA and pure LMA homopolymers. As a reference, the activation energy for viscous flow for many linear polymers is around 25-30kJ/mol. The introduction of high pendant groups or chain branching seems to almost double this value. [52]

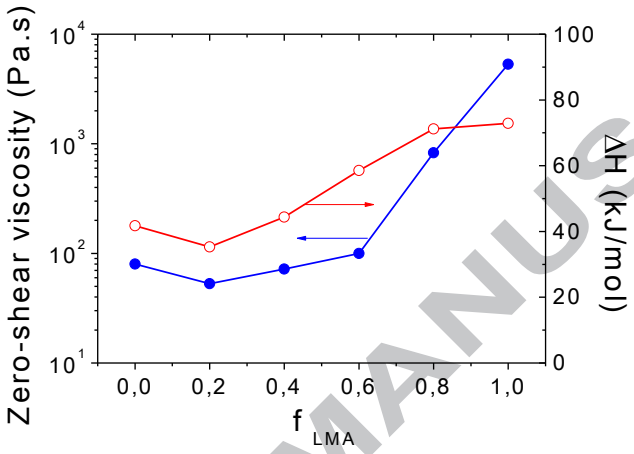

Figure 7. Zero-shear viscosity at 20 ºC and ΔH Arrhenius vs. f_{LMA} for condition 2.

Solution Properties

Surface Tension Analysis

The hydrophilic-lipophilic balance (HLB) is an estimation of the hydrophilic degree of an amphiphilic molecule. This value is determined by calculating values for the different regions of the entity. Several methods are used to determine HLB. According to Griffin's method, the HLB value is dependent on the molecular mass of the hydrophilic portion of the molecule (M_h) with respect to the molecular mass of the whole molecule (M), according to equation 2.[53,54]

$$HLB = 20 * \frac{M_h}{M} \ (eq\ 2)$$

$$HLB = 20 * \frac{0.173 * M_{LMA} * F_{LMA} + 0.888 * M_{PEGMA} * F_{PEGMA}}{M_{LMA} * F_{LMA} + M_{PEGMA} * F_{PEGMA}}$$

In our systems, we considered LMA monomers with 17.3 wt% of hydrophilic region (ester group) and PEGMA monomers with 88.8 wt% of hydrophilic region (all monomers except CH_2 and

C groups of the main chain and terminal CH_3 of pendant group). Table 2 lists the HLB values of all the synthesized copolymers. According to Griffin's method, HLB values less than 10 correspond to water-insoluble systems (experimentally observed for $LMA_{0.8}$-$PEGMA_{0.2}$). HLB values between 8 and 16 correspond to oil/water emulsifying agents. In fact, a water phase can introduce parts of an oil phase. Moreover, if the HLB value is close to 12.5-15, the surfactant could show detergent capability. In this case, we selected three copolymers with HLB values in the aforementioned range ($LMA_{0.4}$-$PEGA_{0.6}$ with and without composition drift and $LMA_{0.6}$-$PEGAM_{0.4}$ with composition drift) one copolymer below the range ($LMA_{0.6}$-$PEGAM_{0.4}$ without composition drift), and one copolymer above the aforementioned range ($LMA_{0.2}$-$PEGAM_{0.8}$ with composition drift). The surface tension as a function of the concentration was determined for the five systems. Figure 8 illustrates the plots obtained.

Table 2. Hydrophilic-lipophilic balance (HLB) estimation for the copolymers synthesized under condition 1 (without composition drift) and condition 2 (with composition drift).

Copolymer	HLB 20% Cu^{II} Condition 1	HLB 0% Cu^{II} Condition 2
$LMA_{0.2}$-$PEGMA_{0.8}$	15.4	***16.1***
$LMA_{0.4}$-$PEGMA_{0.6}$	***12.7***	***14.5***
$LMA_{0.6}$-$PEGMA_{0.4}$	***10.0***	***12.5***
$LMA_{0.8}$-$PEGMA_{0.2}$	7.1	8.6

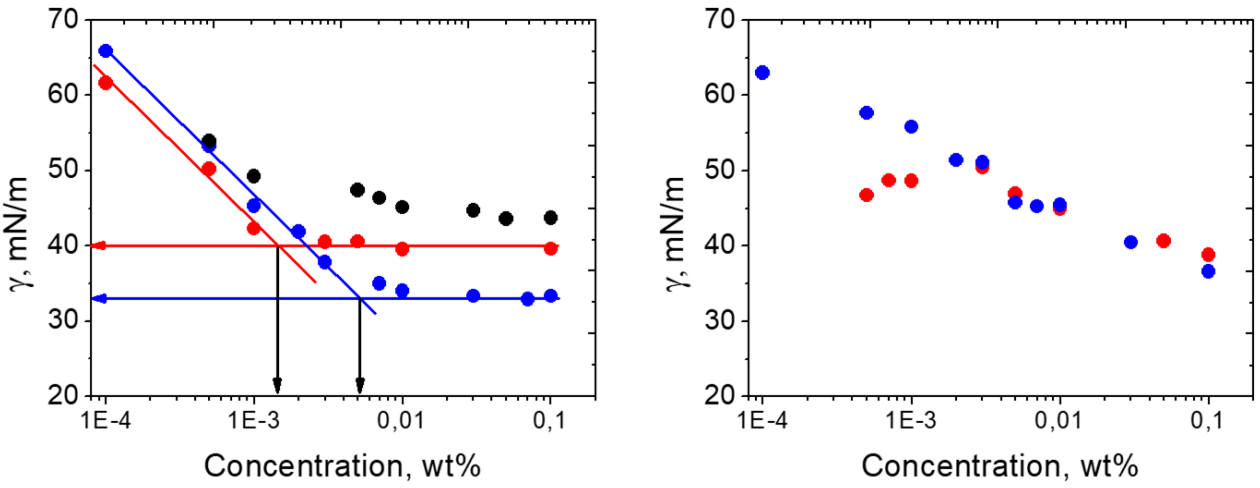

Figure 8. Surface tension values as a function of sample concentration for $LMA_{0.2}$-$PEGMA_{0.8}$ (•), $LMA_{0.4}$-$PEGMA_{0.6}$ (•) and $LMA_{0.6}$-$PEGMA_{0.4}$ (•) in water. Left corresponds to a copolymer without composition drift (condition 1) and right corresponds to a copolymer with composition drift (condition 2).

Figure 8 shows that for all the selected copolymers, the surface tension decreased as the sample concentration increased. This context highlights the surfactant capability of all the copolymers obtained. $LMA_{0.4}$-$PEGMA_{0.6}$ and $LMA_{0.6}$-$PEGMA_{0.4}$ with composition drift (condition 2) showed a clear critical micelle concentration (CMC). CMC is an important characteristic of a surfactant and, before reaching the CMC, the surface tension changes significantly when the surfactant concentration does. After reaching the CMC, the surface tension remains relatively constant or changes with a lower slope. $LMA_{0.2}$-$PEGMA_{0.8}$ did not show major surface tension changes before CMC, probably due to its high solubility in water, as indicated by its HLB.[55,56] As illustrated in figure 8, $LMA_{0.4}$-$PEGMA_{0.6}$ displayed a CMC close to 1.5E-3 wt% and the surface tension value at this concentration was 40 mN/m. On the other hand, $LMA_{0.6}$-$PEGMA_{0.4}$ showed higher CMC than $LMA_{0.4}$-$PEGMA_{0.6}$ (5E-3 wt%), though lower surface tension CMC (33 mN/m). In order to evaluate the surfactants performance, the amount of surfactant adsorbed per unit area of liquid-gas interface was evaluated. This amount was indirectly calculated from the interfacial tension measurements. The concentration of surfactants at the water–air interface can be calculated as the surface excess concentration, ??max (equation 3).[57,58]

??γ/??lnC is the slope of the γ plot versus lnC at constant temperature (T), and R is the gas constant. The surface excess concentration at surface saturation is a useful tool to measure the effectiveness of the surfactant adsorption at the liquid–gas or liquid–liquid interface, since it is the maximum value attainable by adsorption. The area per molecule at the interface provides information on the degree of packing and the orientation of the adsorbed surfactant molecules. From the surface excess concentration, the area per molecule at the interface (*Amin*) is calculated using Equation 4, where N is Avogadro's number.

$$\Gamma max = \frac{1}{2\mathrm{RT}} \times \frac{\partial \gamma}{\partial \ln \mathrm{C}} \text{ (eq 3)} \qquad Amin = \frac{10^{16}}{N} \Gamma max \text{ (eq 4)}$$

The plot for $LMA_{0.4}$-$PEGMA_{0.6}$ yielded an *Amin* value of 0.586 nm^2/molecule of surface area per polymer molecule with an R^2 value of 0.94. On the other hand, the plot for $LMA_{0.6}$-$PEGMA_{0.4}$ revealed an *Amin* value of 0.499 nm^2/molecule of surface area per polymer molecule with an R^2 value of 0.99. Even though *Amin* values are quite similar, they reveal the dependence of the adsorption effectiveness on surfactants structure in the aqueous solution–air interfaces. The higher

amount of lipophilic entity in the $LMA_{0.6}$-$PEGMA_{0.4}$ copolymer produced a higher packing in this copolymer. On the other hand, $LMA_{0.4}$-$PEGMA_{0.6}$ featured a more expanded structure due to its higher hydrophilic monomer content.

$LMA_{0.4}$-$PEGMA_{0.6}$ and $LMA_{0.6}$-$PEGMA_{0.4}$, without composition drift (condition 1), did not show a *plateau* in the surface tension. Despite the surfactant capability of these copolymers, their performance was far from satisfactory, and probably they would not be optimal for use in the surfactant field, as demonstrated below. $LMA_{0.4}$-$PEGMA_{0.6}$ showed an increase in surface tension at low concentrations, due to its high solubility in water at said concentrations. Then, it displayed a continuous decrease in surface tension as a function of its concentration. This second behavior, observed along all the concentration range of $LMA_{0.6}$-$PEGMA_{0.4}$, is common for compounds with a noticeable nonpolar contribution, as indicated by the HLB; and the continuous decrease in surface tension is explained by the continuous accumulation of molecules on the surface.[59]

Emulsification studies and characterization of aggregates

In order to evaluate the nonionic-emulsifying properties, toluene was incorporated into aqueous solutions of $LMA_{0.4}$-$PEGMA_{0.6}$ and $LMA_{0.6}$-$PEGMA_{0.4}$ copolymers. Table 3 lists the different DLS sizes (in number and distribution fit) of the aqueous solutions of the aforementioned copolymers (with and without composition drift), and of these solutions with 2% of toluene. Size evolution shows a clear difference with respect to copolymer composition and microstructure. Copolymers without composition drift (condition 1) featured particle sizes of 55 and 99 nm for $LMA_{0.4}$-$PEGMA_{0.6}$ and $LMA_{0.6}$-$PEGMA_{0.4}$, respectively. In this case, toluene incorporation produced an increase in particle size to 106 and 126 nm, for $LMA_{0.4}$-$PEGMA_{0.6}$ and $LMA_{0.6}$-$PEGMA_{0.4}$, respectively. On the contrary, copolymers with composition drift (condition 2), showed smaller sizes of 10 and 15 nm for $LMA_{0.4}$-$PEGMA_{0.6}$ and $LMA_{0.6}$-$PEGMA_{0.4}$, respectively, and toluene incorporation led to the formation of particles with sizes of 154 and 42 nm, for $LMA_{0.4}$-$PEGMA_{0.6}$ and $LMA_{0.6}$-$PEGMA_{0.4}$, respectively. The different aggregate sizes revealed interesting observations about the effect of copolymer microstructure. Regarding the size of aggregates in water, the system without composition drift showed larger sizes than the system with drift. The homopolymer domain in the copolymer microstructure (copolymers with drift) produced a decrease in particle size due to an increase in the monomer-monomer interaction. Comparisons between aggregate sizes of statistical and block copolymers support this suggestion.[60] Both microstructures displayed an increase in particle size in water when the LMA content increased. Reasonably, the content of the hydrophobic monomer expanded the particle size due to the increase in the amount of LMA inside the aggregates. The incorporation of toluene in the copolymer solutions led to particle size expansion in all cases due

to the toluene load inside the particle. The copolymers with lowest LMA content ($LMA_{0.4}$-$PEGMA_{0.6}$) produced greater size expansion due to the incorporation of toluene when composition drift was present. According to the HBL value, a greater hydrophilic content presumed a larger particle size. The $LMA_{0.6}$-$PEGMA_{0.4}$ system with composition drift produced an expansion of three times its size, as compared to $LMA_{0.4}$-$PEGMA_{0.6}$ without drift, with similar HBL values. The $LMA_{0.6}$-$PEGMA_{0.4}$ system without composition drift was the system with the lowest particle growth due to toluene addition, a behavior opposite to that of $LMA_{0.4}$-$PEGMA_{0.6}$ with drift and in line with its HLB values.

Table 3. DLS aggregate sizes based on $LMA_{0.4}$-$PEGMA_{0.6}$ and $LMA_{0.6}$-$PEGMA_{0.4}$ with different microstructure. Size modification due to toluene incorporation. Polymer concentration was $1 g.L^{-1}$ and the emulsification studies incorporate 2% of toluene.

Copolymer	Condition	Aggregate sizes in water (nm)	Aggregate sizes with toluene (nm)
$LMA_{0.4}$-$PEGMA_{0.6}$	**20% Cu^{II} (Condition 1)**	55±18	106±39
	0% Cu^{II} (Condition 2)	10±2	154±43
$LMA_{0.6}$-$PEGMA_{0.4}$	**20% Cu^{II} (Condition 1)**	99±33	126±55
	0% Cu^{II} (Condition 2)	15±3	42±8

The comparison of CMC values and DLS sizes for copolymers with compositional drift (condition 2), showed correlated results: $LMA_{0.4}$-$PEGMA_{0.6}$ showed a CMC close to 1.5E-3 wt% with an aggregate size average of 10 nm. On the other hand, $LMA_{0.6}$-$PEGMA_{0.4}$ showed a higher CMC (5E-3 wt%) value and higher aggregate sizes (average of 15 nm) than $LMA_{0.4}$-$PEGMA_{0.6}$. For condition 1, copolymers without compositional drift, the systems did not show CMC and the aggregates evaluated by DLS were larger because they were not hierarchically formed, and their hydrodynamic size was greater than that of copolymers under condition 2, with a high standard deviation (monomodal profile).

In order to corroborate the encapsulation of toluene into the copolymer aggregates, Diffusion-Ordered Spectroscopy NMR (DOSY-NMR) measurements were carried out in copolymer samples

with 2% of toluene (figure 9). Figure 9a corresponds to $LMA_{0.6}$-$PEGMA_{0.4}$ without composition drift (20% Cu^{II} – Condition 1), and figure 9b to that same copolymer with composition drift (0% Cu^{II} – Condition 2). Toluene spectra were superimposed for comparison (red signals). The value of the diffusion constants of toluene associated with the copolymers was more similar to that of the copolymers for $LMA_{0.6}$-$PEGMA_{0.4}$ with composition drift (figure 9b). The diffusion constants of both signals, the aromatic around 7 ppm and the methyl group at 2 ppm were in the range of copolymer values of -10 m^2/s. In the case of $LMA_{0.6}$-$PEGMA_{0.4}$ without composition drift (figure 9a), the similarity in diffusion constants is not that clear. These differences are in agreement with the emulsion aspect (figure 10a). Finally, and in order to clarify and better understand the interactions between toluene molecules within copolymer aggregates, Nuclear Overhauser Effect NMR spectroscopy (NOESY-NMR) measurements were taken. Figures 9c and 9d illustrate the spectra of $LMA_{0.6}$-$PEGMA_{0.4}$ without (20% Cu^{II} – Condition 1) and with (0% Cu^{II} – Condition 2) composition drift, respectively. The cross-correlation peaks of the aromatic signals of toluene and methylene groups of LMA monomer (signal *d* in figure 1) at 1.25 ppm assume the interaction between copolymers and toluene, and the interaction is more clear in the case of $LMA_{0.6}$-$PEGMA_{0.4}$ with composition drift (0% Cu^{II} – Condition 2, figure 9d). According to DOSY results, in the case of $LMA_{0.6}$-$PEGMA_{0.4}$ without composition drift (figure 9c), cross-correlation peaks were not that clear. This context assumes a better capacity of $LMA_{0.6}$-$PEGMA_{0.4}$ with composition drift than of $LMA_{0.6}$-$PEGMA_{0.4}$ without composition drift to encapsulate toluene in the aggregate structures.

As shown in Figure 9, the diffusion coefficient of toluene in the presence of the copolymer lies between the free toluene without copolymer and the copolymer itself. This is probably due to the fact that toluene is partitioned between water and the polymer, and so the value measured corresponds to the average of the extreme values of the diffusion coefficient.

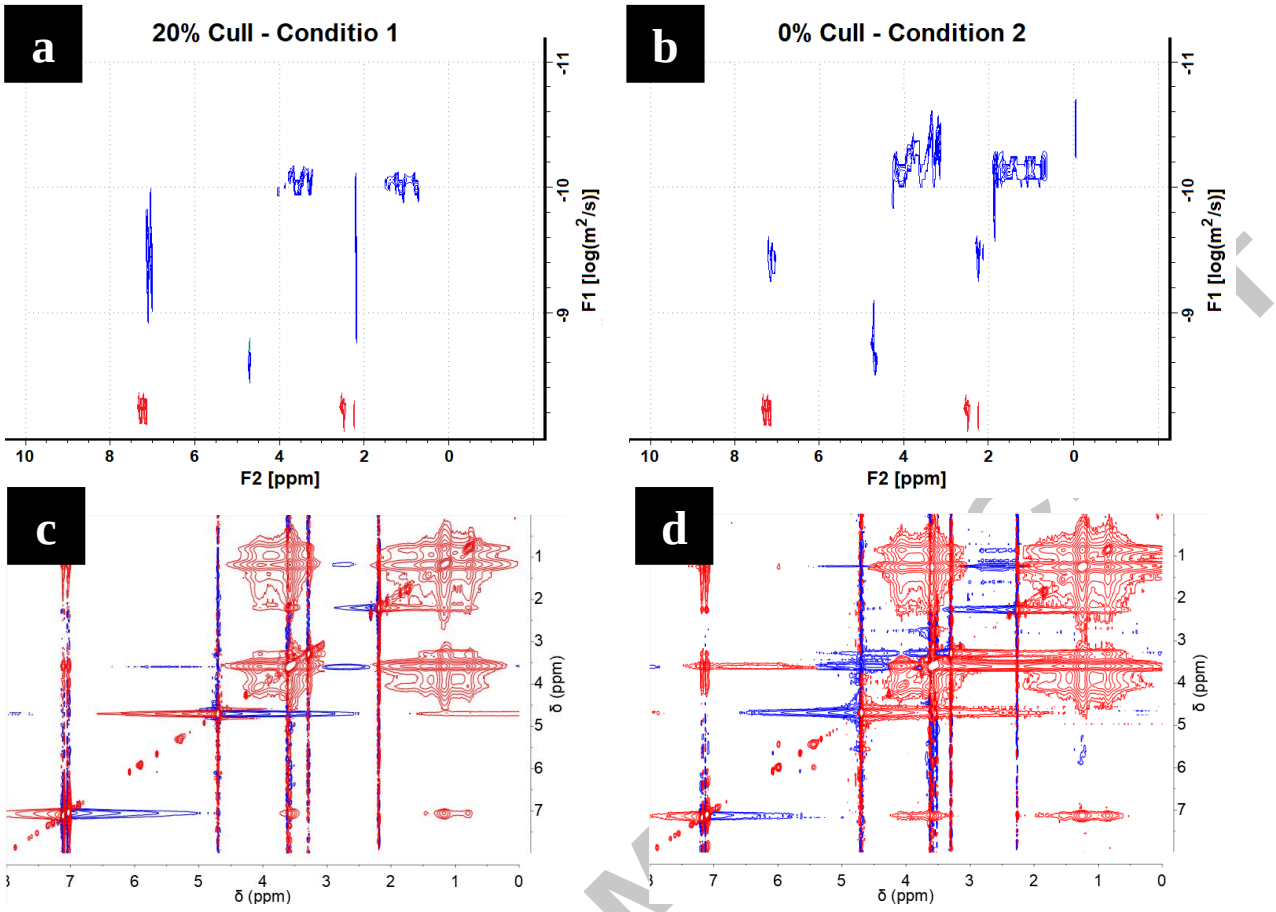

Figure 9. DOSY NMR spectra of solution in presence of toluene of $LMA_{0.6}$-$PEGMA_{0.4}$ without composition drift (a) and with composition drift (b). c and d are the NOESY-NMR spectra corresponding to a and b systems, respectively.

Finally, figure 10a shows a photograph of $LMA_{0.6}$-$PEGMA_{0.4}$ dispersion with and without composition drift. The image displays the better capacity that $LMA_{0.6}$-$PEGMA_{0.4}$ with composition drift (0% Cu^{II} – Condition 2) has to stabilize toluene. $LMA_{0.6}$-$PEGMA_{0.4}$ without composition (20% Cu^{II} – Condition 1) showed greater turbidity, due to the greater hydrophobic nature of the system (copolymer + toluene) and larger particle size as was observed by DLS. Figure 10b illustrates an AFM micrograph of $LMA_{0.6}$-$PEGMA_{0.4}$ with composition drift, the selected candidate with the best conditions to emulsify toluene. The figure confirms that the aggregate size is around 40 nm. As expected, the aggregate sizes obtained by AFM are lower than the values obtained by DLS due to the measurement conditions, DLS determinations were performed in water dispersions and AFM determinations were performed in dry conditions.

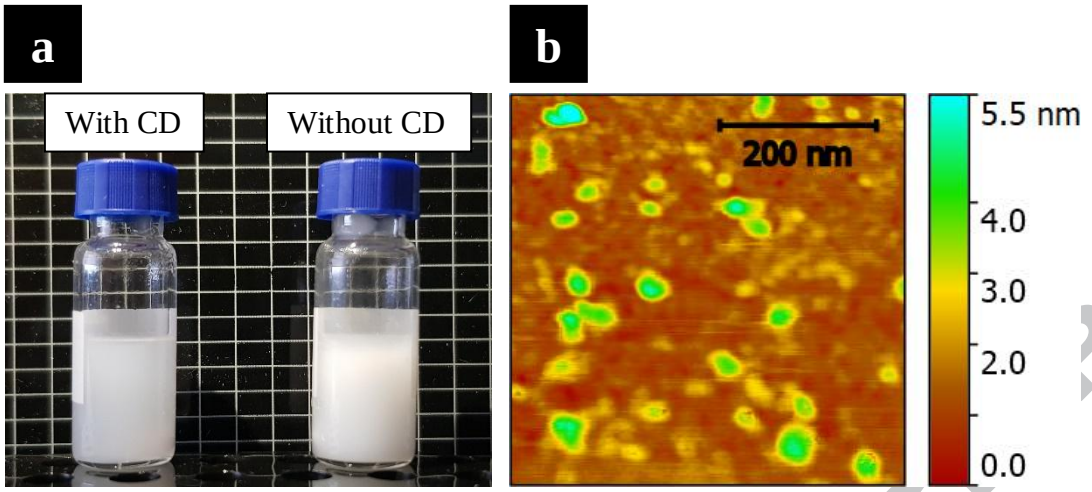

Figure 10. (a) Dispersion of $LMA_{0.6}$-$PEGMA_{0.4}$ with (left) and without (right) composition drift and (b) AFM micrograph of $LMA_{0.6}$-$PEGMA_{0.4}$ with composition drift.

The present work describes a complete and thorough synthesis and thermal and rheological characterization of copolymers based on lauryl methacrylate and poly(ethylene glycol) methyl ether methacrylate. The obtained results show a clear amphiphilic capacity of a limited range of these copolymers with different compositions and microstructures. The aggregate sizes showed remarkable differences and the copolymer $LMA_{0.6}$-co-$PEGMA_{0.4}$ with composition drift was the best copolymer to incorporate toluene and produce aggregates of approximately 45 nm in size. Composition and microstructure are crucial factors to better understand the physical-chemistry of emulsifying systems.

CONCLUSIONS

The of copolymers based on lauryl methacrylate and poly(ethylene glycol) methyl ether methacrylate was described. Thermal and rheological properties showed a clear effect on transitions when composition drift was present. The emulsifying properties of the prepared systems depend both on their copolymer composition and on their microstructure. Copolymers in a intermediate composition range displayed adequate hydrophilic-lipophilic balance as emulsifying agents and, particularly, some of them showed detergency properties. The surface tension analysis revealed better emulsifying properties in the systems with composition drift; and dynamic light scattering showed smaller sizes for aggregates in these systems. Self-assembled aggregates characterization using Diffusion-Ordered Spectroscopy NMR, Nuclear Overhauser Effect NMR spectroscopy, and Atomic Force Microscopy showed that $LMA_{0.6}$-co-$PEGMA_{0.4}$ with composition drift is the best candidate to emulsify an organic phase in water.

REFERENCES

1 F. Safaei, S. N. Khorasani, H. Rahnama, R. E. Neisiany and M. S. Koochaki, *Prog. Org. Coatings*, 2018, **114**, 40–46.

2 Z. Flores, D. San Martín, R. Villalobos-Carvajal, G. Tabilo-Munizaga, F. Osorio and J. Leiva-Vega, *Food Hydrocoll.*, 2016, **61**, 851–857.

3 L. Sen Lin, X. Yang, G. Niu, J. Song, H. H. Yang and X. Chen, *Nanoscale*, 2016, **8**, 2116–2122.

4 Z. Fakhravar, P. Ebrahimnejad, H. Daraee and A. Akbarzadeh, *Nanoliposomes: Synthesis methods and applications in cosmetics*, 2016, vol. 18.

5 A. Ferreira, X. Vecino, D. Ferreira, J. M. Cruz, A. B. Moldes and L. R. Rodrigues, *Colloids Surfaces B Biointerfaces*, 2017, **155**, 522–529.

6 A. Gharsallaoui, G. Roudaut, O. Chambin, A. Voilley and R. Saurel, *Food Res. Int.*, 2007, **40**, 1107–1121.

7 E. Dickinson, *Food Hydrocoll.*, 2009, **23**, 1473–1482.

8 I. Kralova and J. Sjöblom, *J. Dispers. Sci. Technol.*, 2009, **30**, 1363–1383.

9 F. J. Tölle, M. Fabritius and R. Mülhaupt, *Adv. Funct. Mater.*, 2012, **22**, 1136–1144.

10 J. Su, L. Wang and L. Ren, *J. Appl. Polym. Sci.*, 2006, **101**, 1522–1528.

11 G. Bognolo, *Colloids Surfaces A Physicochem. Eng. Asp.*, 1999, **152**, 41–52.

12 J. Falcon Hernandez and J. Carbonell Morla, *Energy & Fuels*, 2003, **17**, 302–307.

13 N. Zaki, T. Butz and D. Kessel, *Pet. Sci. Technol.*, 2001, **19**, 425–435.

14 J. B. Zimmerman, A. F. Clarens, K. F. Hayes and S. J. Skerlos, *Environ. Sci. Technol.*, 2003, **37**, 5278–5288.

15 A. M. Mathur, B. Drescher, A. B. Scranton and J. Klier, *Nature*, 1998, **392**, 367–370.

16 S. Fujii, Y. Cai, J. V. M. Weaver and S. P. Armes, *J. Am. Chem. Soc.*, 2005, **127**, 7304–7305.

17 G. Riess, J. Nervo and D. Rogez, *Polym. Eng. Sci.*, 1977, **17**, 634–638.

18 B. Brugger and W. Richtering, *Langmuir*, 2008, **24**, 7769–7777.

19 J. W. Anseth, A. Bialek, R. M. Hill and G. G. Fuller, *Langmuir*, 2003, **19**, 6349–6356.

20 P. M. Claesson, R. Makuska, I. Varga, R. Meszaros, S. Titmuss, P. Linse, J. S. Pedersen and C. Stubenrauch, *Adv. Colloid Interface Sci.*, 2010, **155**, 50–57.

21 P. Chambon, A. Chemtob, E. Cloutet, H. Cramail, S. Gibanel, Y. Gnanou, V. Héroguez, D. Quéméner and B. Radhakrishnan, *Polym. Int.*, 2006, **55**, 1146–1154.

22 P. Viswanathan, E. Themistou, K. Ngamkham, G. Reilly, S. P. Armes and G. Battaglia, *Biomacromolecules*, 2014, **16**, 66–75.

23 X. G. Qiao, P. Y. Dugas, B. Charleux, M. Lansalot and E. Bourgeat-Lami, *Macromolecules*, 2015, **48**, 545–556.

24 M. Stefik, J. Song, H. Sai, S. Guldin, P. Boldrighini, M. C. Orilall, U. Steiner, S. M. Gruner and U. Wiesner, *J. Mater. Chem. A*, 2015, **3**, 11478–11492.

25 L. Chen, T. Ci, T. Li, L. Yu and J. Ding, *Macromolecules*, 2014, **47**, 5895–5903.

26 J. Zhou, L. Wang, C. Wang, T. Chen, H. Yu and Q. Yang, *Polymer (Guildf).*, 2005, **46**, 11157–11164.

27 L. Gargallo, A. Opazo and D. Radic, *Eur. Polym. J.*, 1990, **26**, 727–730.

28 A. Leiva, L. Gargallo and D. Radic, *J. Macromol. Sci. Part B*, 1998, **37**, 45–57.

29 H. Ahmad, M. K. Hasan, M. A. J. Miah, A. M. I. Ali and K. Tauer, *Polymer (Guildf).*, 2011, **52**, 3925–3932.

30 A. Matsumoto, N. Murakami, H. Aota, J. Ikeda and I. Capek, *Polymer (Guildf).*, 1999, **40**, 5687–5690.

31 A. Iborra, G. Díaz, D. López, J. M. Giussi and O. Azzaroni, *Eur. Polym. J.*, 2017, **87**, 308–317.

32 Y. Xia, B. D. Olsen, J. A. Kornfield and R. H. Grubbs, *J. Am. Chem. Soc.*, 2009, **131**, 18525–18532.

33 D. Gromadzki, P. Štěpánek and R. Makuška, *Mater. Chem. Phys.*, 2013, **137**, 709–715.

34 J. Pietrasik, B. S. Sumerlin, R. Y. Lee and K. Matyjaszewski, *Macromol. Chem. Phys.*, 2007, **208**, 30–36.

35 S. I. Yamamoto, J. Pietrasik and K. Matyjaszewski, *Macromolecules*, 2008, **41**, 7013–7020.

36 S. I. Yamamoto, J. Pietrasik and K. Matyjaszewski, *Macromolecules*, 2007, **40**, 9348–9353.

37 K. Matyjaszewski, M. J. Ziegler, S. V. Arehart, D. Greszta and T. Pakula, *J. Phys. Org. Chem.*, 2000, **13**, 775–786.

38 H. A. S. Schoonbrood, H. M. G. Brouns, H. A. Thijssen, A. M. Van Herk and A. L. German, *Macromol. Symp.*, 1995, **156**, 133–156.

39 C. L. McCormick and C. B. Johnson, *Macromolecules*, 1988, **21**, 686–693.

40 G. Odian, *Principles of Polymerization*, John Wiley & Sons, Inc., New York, 4th Edition, 2004.

41 E. D. Goddard, *Colloids and Surfaces*, 1986, **19**, 255–300.

42 C. Methemitis, M. Morcellet, J. Sabbadin and J. Francois, *Eur. Polym. J.*, 1986, **22**, 619–627.

43 J. C. Brackman, B. Jan and N. Engberts, *J. Am. Chem. Soc.*, 1990, **112**, 872–873.

44 a P. Mast, R. K. Prudhomme and J. E. Glass, *Langmuir*, 1993, **9**, 708–715.

45 B. Magny, I. Iliopoulos, R. Zana and R. Audebert, *Langmuir*, 1994, **10**, 3180–3187.

46 T. Annable, R. Buscall and R. Ettelaie, *Langmuir*, 1994, **10**, 1060–1070.

47 H. M. Kopperud, F. K. Hansen and B. Nystrom, *Macromol Chem. Phys.*, 1998, **2394**, 2385–2394.

48 J. A. Jones, N. Novo, K. Flagler, C. D. Pagnucco, S. Carew, C. Cheong, X. Z. Kong, N. A. D. Burke and H. D. H. Stöver, *J. Polym. Sci. Part A Polym. Chem.*, 2005, **43**, 6095–6104.

49 D. Neugebauer, Y. Zhang and T. Pakula, *J. Polym. Sci. Part A Polym. Chem.*, 2006, **44**, 1347–1356.

50 J. M. Giussi, I. Blaszczyk-Lezak, B. Sanz, P. E. Allegretti, C. Mijangos and M. S. Cortizo, *Eur. Polym. J.*, 2014, **59**, 84–93.

51 P. S. Vijayanand, S. Kato, S. Satokawa, M. Kishimoto and T. Kojima, *React. Funct. Polym.*, 2009, **69**, 333–340.

52 C.W. Macosko, *Rheology: Principles, Measurements and Applications*, Wiley-VCH, New York, 1994.

53 J. Hu, Z. Jin, T. Y. Chen, J. D. Polley, M. F. Cunningham and R. A. Gross, *Macromolecules*,

2014, **47**, 113–120.

54 S. W. An, R. K. Thomas, C. Forder, N. C. Billingham, S. P. Armes and J. Penfold, *Langmuir*, 2002, **18**, 5064–5073.

55 J. B. Vieira, Z. X. Li and R. K. Thomas, *J. Phys. Chem. B*, 2002, **106**, 5400–5407.

56 F. Yang and M. Hai, *J. Chem. Eng. Data*, 2013, **58**, 2051–2057.

57 B. Jańczuk, A. Zdziennicka and W. Wójcik, *Colloids and Surfaces A: Physicochemical and Engineering Aspects*, 2003, **220,** 61-68.

58 A. M. Atta, S. I. El-Sherbiny, A. M. Salah and A. R. Abd El-hafiez Ahmed, *Journal of Dispersion Science and Technology*, 2013, **34,** 1113-1123.

59 B. Rippner, K. Boschkova, P. M. Claesson and T. Arnebrant, *Langmuir*, 2002, **18**, 5213–5221.

60 C. G. Bell, C. J. W. Breward, P. D. Howell, J. Penfold, R. K. Thomas, V. Uni and S. Giles, *Langmuir*, 2007, **23**, 6042–6052.

HIGHLIGHTS

- Controlled synthesis of non-ionic amphiphilic copolymer based on lauryl methacrylate and Poly(ethylene glycol) methyl ether methacrylate.
- Effect of compositional drift in thermal and emulsifier properties.
- Interesting bulk rheological properties.
- Incorporation of toluene in formed micelles. Evaluation of loading capacity using 2D NMR

Graphical Abstract